nature geoscience

Article

https://doi.org/10.1038/s41561-023-01345-6

Relative increases in CH_4 and CO_2 emissions from wetlands under global warming dependent on soil carbon substrates

Received: 15 February 2023

Accepted: 31 October 2023

Published online: 3 January 2024

Check for updates

Han Hu[1,2,13], Ji Chen[3,4,5,13], Feng Zhou[6], Ming Nie[7], Deyi Hou[8], Huan Liu[8], Manuel Delgado-Baquerizo[9], Haowei Ni[1,2], Weigen Huang[1,2], Jizhong Zhou[10], Xianwei Song[11], Xiaofeng Cao[11], Bo Sun[1], Jiabao Zhang[1], Thomas W. Crowther[12] & Yuting Liang[1,2]

Compelling evidence has shown that wetland methane emissions are more temperature dependent than carbon dioxide emissions across diverse hydrologic conditions. However, the availability of carbon substrates, which ultimately determines microbial carbon metabolism, has not been adequately accounted for. By combining a global database and a continental-scale experimental study, we showed that differences in the temperature dependence of global wetland methane and carbon dioxide emissions ($E_{M/C}$) were dependent on soil carbon-to-nitrogen stoichiometry. This can be explained mainly by the positive relationship between soil organic matter decomposability and $E_{M/C}$. Our study indicates that only 23% of global wetlands will decrease methane relative to carbon dioxide emissions under future warming scenarios when soil organic matter decomposability is considered. Our findings highlight the importance of incorporating soil organic matter biodegradability into model predictions of wetland carbon–climate feedback.

Wetlands store 29–45% of terrestrial soil organic carbon (SOC)[1,2]. Methane (CH_4) and carbon dioxide (CO_2) are the dominant gaseous products of wetland SOC decomposition[3] as well as the main causes of climate change characterized primarily by global warming[4]. Since CH_4 has at least a 28-fold global warming potential compared with CO_2 (refs. 5,6), the relative emissions of CH_4 to CO_2 are a prominent determinant of the climate-forcing effect on greenhouse gas emissions in wetlands[3,7]. The temperature dependence of CH_4 and CO_2 emissions can be described by the apparent activation energies (E_M and E_C), and their difference can be expressed as $E_{M/C}$ (refs. 3,8). A positive $E_{M/C}$ implies that CH_4 emissions are more sensitive to temperature change than CO_2 emissions, which indicates that the relative emissions of CH_4 to CO_2 increase under warming conditions. In the face of irreversible global warming, identifying the drivers of $E_{M/C}$ is important for predicting the warming effects on greenhouse gas emissions in wetlands.

[1]State Key Laboratory of Soil and Sustainable Agriculture, Institute of Soil Science, Chinese Academy of Sciences, Nanjing, China. [2]University of the Chinese Academy of Sciences, Beijing, China. [3]State Key Laboratory of Loess and Quaternary Geology, Institute of Earth Environment, Chinese Academy of Sciences, Xi'an, China. [4]Department of Agroecology, Aarhus University, Tjele, Denmark. [5]iCLIMATE Interdisciplinary Centre for Climate Change, Aarhus University, Roskilde, Denmark. [6]College of Urban and Environmental Sciences, Peking University, Beijing, China. [7]School of Life Sciences, Fudan University, Shanghai, China. [8]State Key Joint Laboratory of ESPC, School of the Environment, Tsinghua University, Beijing, China. [9]Laboratorio de Biodiversidad y Funcionamiento Ecosistémico, Instituto de Recursos Naturales y Agrobiología de Sevilla (IRNAS), CSIC, Sevilla, Spain. [10]School of Biological Sciences, University of Oklahoma, Norman, OK, USA. [11]State Key Laboratory of Plant Genomics and National Center for Plant Gene Research (Beijing), Institute of Genetics and Developmental Biology, Chinese Academy of Sciences, Beijing, China. [12]Department of Environmental Systems Science, Institute of Integrative Biology, ETH, Zurich, Switzerland. [13]These authors contributed equally: Han Hu, Ji Chen. e-mail: ytliang@issas.ac.cn

https://doi.org/10.1038/s41561-023-01345-6

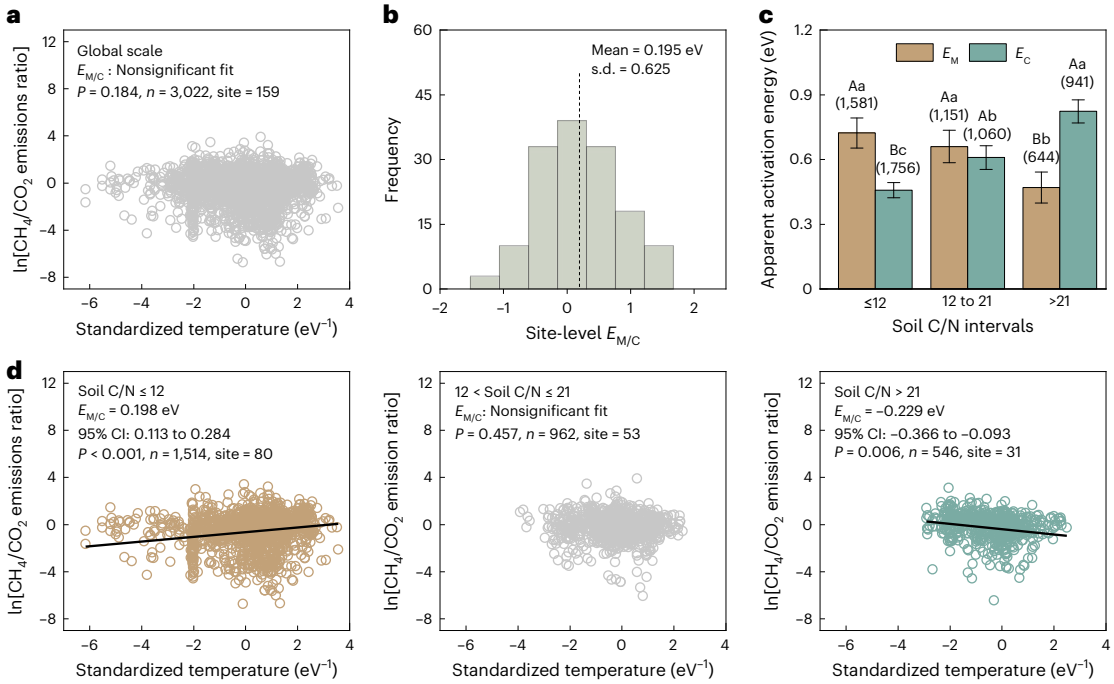

Fig. 1 | Temperature dependence of the CH_4/CO_2 emissions ratio ($E_{M/C}$). **a**, The $E_{M/C}$ on a global scale. The temperature dependence of the greenhouse gas emissions was characterized using the LME model after fitting the Boltzmann–Arrhenius function to the data of the CH_4/CO_2 emissions ratios and the standardized temperature (Methods). **b**, The $E_{M/C}$ at the site level. The dashed line indicates the average value. **c**, Temperature dependence of E_M and E_C. The numbers in parentheses represent the sample sizes. The data are presented as the mean ± the standard error (the standard error values were obtained from the LME models). Different capital letters denote significant differences between different greenhouse gas types at the same soil C/N interval ($P < 0.05$). Different lowercase letters denote significant differences between different soil C/N intervals of the same greenhouse gas type ($P < 0.05$). The classification of different soil C/N intervals was based on the results of Supplementary Table 2. **d**, The $E_{M/C}$ at different soil C/N intervals. The $E_{M/C}$ was characterized using the LME model.

A growing body of research suggests that the proportional emissions of CH_4 from wetlands are increasing under warming conditions relative to CO_2, with the potential to accelerate positive feedback to climate warming[3,8]. However, the majority of previous studies have focused primarily on the effects of hydrological changes, suggesting that wetland hydrological conditions might be the most important factor driving variations in $E_{M/C}$ (refs. 3,9–12). As such, it has been reported that wetland $E_{M/C}$ shifts from positive to negative with the decline in water-table depth (WTD) across the globe[3]. This is due to the change in oxygen content caused by WTD fluctuation, which affects the production and oxidation of methane[13–15]. However, the wetland $E_{M/C}$ is not only subject to hydrological conditions[8] but also fundamentally underpinned by the availability of carbon substrate[16–18]. The temperature dependencies of CH_4 and CO_2 emissions may be closely related to the decomposability of soil organic matter (SOM). In wetland ecosystems, the majority of CH_4 efflux and more than 70% of soil CO_2 efflux originate from the decomposition of organic matter by soil microorganisms[16–18]. As carbon and nitrogen are the main energy and material sources of soil microorganisms, C/N stoichiometry plays a very important role in microbial metabolism[19,20]. The synthesis of extracellular enzymes for the decomposition of organic carbon by microorganisms depends on the content of available nitrogen in soil[20]. Therefore, the C/N stoichiometry in wetland soil is closely associated with SOM decomposability[19,20], which may affect CH_4 and CO_2 emissions and their temperature dependence[8,21].

Production of CH_4 is more dependent on easily decomposed organic matter than is CO_2 production under climate warming[22,23]. In soils with a low C/N, SOM usually contains more-easily decomposed carbon molecules[24]. Thus, wetland soils with a low C/N ratio may potentially favour a higher relative contribution of CH_4 to greenhouse gas emissions under warming. Given the importance of soil carbon availability in determining soil microbial decomposition pathways in wetlands, the absence of this variation will probably contribute to considerable uncertainty in our understanding of $E_{M/C}$ across the globe. This information is essential if we are to generate a general basis for predicting the strength of climate warming–CH_4 feedbacks in global wetlands.

$E_{M/C}$ depends on soil C/N

To determine whether soil C/N affects global variations in seasonal $E_{M/C}$, we compiled a database comprising 3,022 paired observations of CO_2 and CH_4 emissions from 159 field sites worldwide (Extended Data Fig. 1), covering a very wide range of soil C/N (1 to 72) and diverse subsurface hydrological conditions. We evaluated the apparent activation energy of CO_2 (E_C) and CH_4 (E_M) emissions in the global database. Across this database, global wetland CO_2 and CH_4 emission rates exponentially increased with seasonal temperature ($P < 0.001$; Supplementary Fig. 1)[8,25,26]. E_C and E_M were calculated by the Boltzmann–Arrhenius function using a linear mixed-effects (LME) model[27,28] with temperature as a fixed effect and site as a random effect on the slope and intercept[3,8] (Supplementary Table 1). The results showed that the seasonal E_M (0.65 eV, 95% confidence interval (CI): 0.56 to 0.73) did not differ significantly from the seasonal E_C (0.61 eV, 95% CI: 0.56 to 0.66) on a global scale (Extended Data Fig. 2). Thus, ratios of CH_4 to CO_2 emissions cannot be significantly fitted to temperature at the global scale ($P = 0.184$; Fig. 1a). The frequency distribution of the site-level $E_{M/C}$ could be characterized by a Gaussian distribution, yielding an average temperature dependence of 0.195 eV on a global scale (Fig. 1b). However, when we considered the variation in soil carbon availability, we were able to capture a meaningful proportion of the variations in $E_{M/C}$ across different regions. Specifically, the $E_{M/C}$ can be well fitted at

https://doi.org/10.1038/s41561-023-01345-6

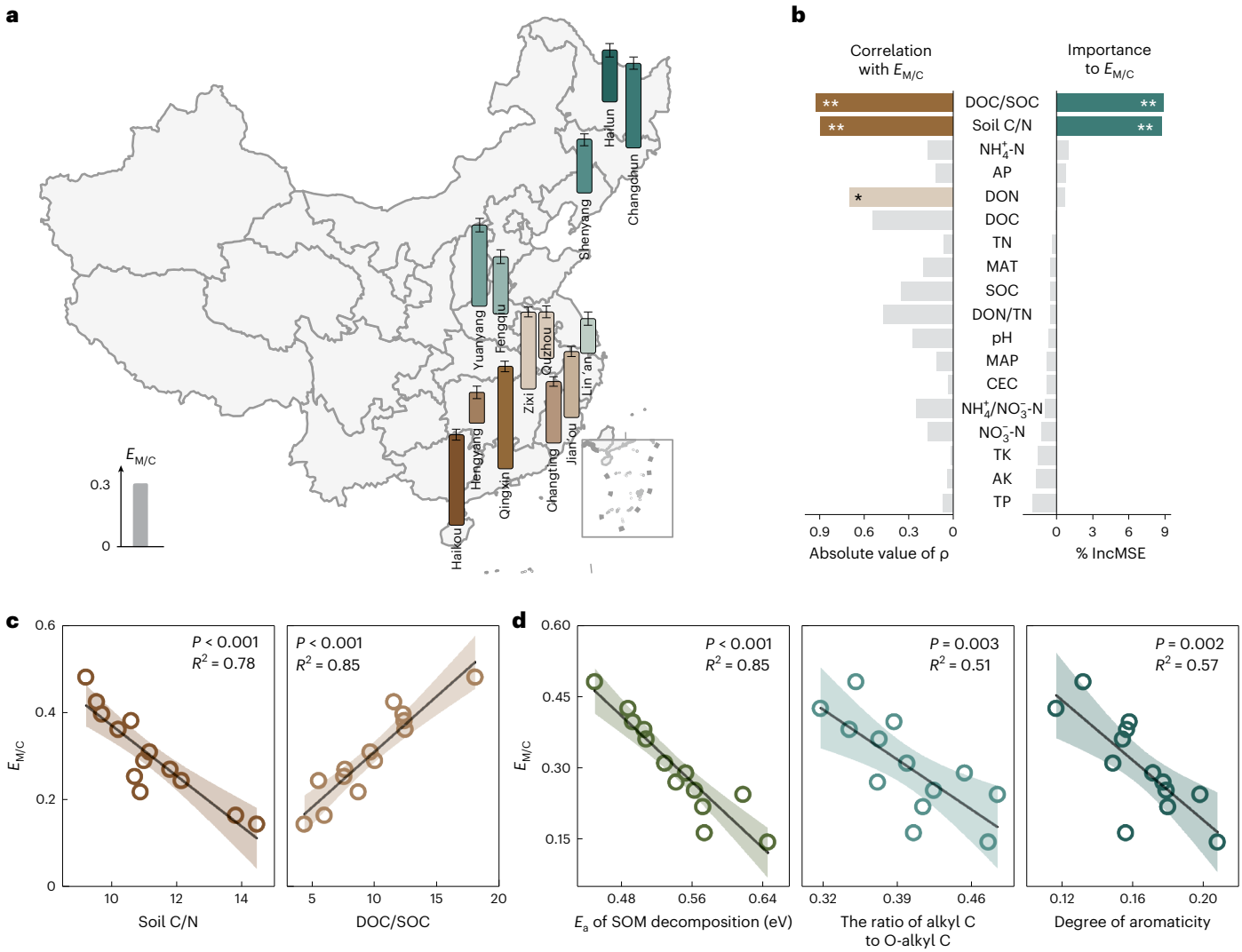

Fig. 2 | Relationships between the temperature dependence of the CH_4/CO_2 emissions ratio ($E_{M/C}$) and SOM decomposability in our incubation experiments. a, Values of $E_{M/C}$ for soils from 13 regions of China from north to south ($n = 3$). The $E_{M/C}$ values were calculated by the difference in the apparent activation energies of E_M and E_C. Error bars are the standard errors of the means. Please refer to Supplementary Figs. 3 and 4 for the E_M and E_C, respectively. **b**, Relationship between $E_{M/C}$ and soil physical and chemical properties by Spearman's correlation analysis and random forest analysis. *Significance at the $P < 0.05$ level; **significance at the $P < 0.01$ level. ρ, Spearman rank correlation coefficient. See Methods for the variables referred to by abbreviations. **c**,**d**, Linear regression analysis between $E_{M/C}$ and soil C/N, the DOC/SOC ratio, the E_a of SOM decomposition, the ratio of alkyl carbon and alkoxy carbon and the degree of aromaticity. Error bands are 95% confidence intervals of the regression lines. The P values for these five linear fits are 3.94×10^{-5}, 4.55×10^{-6}, 3.94×10^{-6}, 3.46×10^{-3} and 1.75×10^{-3} in order. AK, available potassium; AP, available phosphorus; CEC, cation exchange capacity; DON, dissolved organic nitrogen; MAP, mean annual precipitation; MAT, mean annual temperature; TK, total potassium.

different soil C/N intervals by sliding window analysis (Supplementary Table 2). As such, $E_{M/C}$ was positive, with E_M (0.72 eV, 95% CI: 0.59 to 0.86) higher than E_C (0.46 eV, 95% CI: 0.39 to 0.53) when soil C/N was lower than 12. By contrast, $E_{M/C}$ was negative, with E_M (0.47 eV, 95% CI: 0.33 to 0.61) lower than E_C (0.82 eV, 95% CI: 0.72 to 0.93) when soil C/N was higher than 21 (Fig. 1c,d).

Since hydrologic conditions are reported to affect $E_{M/C}$ (ref. 3), we then compared the effects of soil C/N and WTD on the site-level $E_{M/C}$. Soil C/N and WTD did not have multicollinearity for site-level $E_{M/C}$ (Supplementary Table 3). We then used variance partition analysis to show that the relative importance of soil C/N (76.0%) was higher than that of WTD (2.1%; Supplementary Table 3). This result was supported by the optimal model of stepwise regression by comparing the Akaike information criterion values of all possible models (Supplementary Table 4). In addition, a recent study showed that $E_{M/C}$ was positive when WTD was larger than −5 cm and negative when WTD was below −30 cm (ref. 3). We further evaluated the relationship between $E_{M/C}$ and soil C/N under different WTD intervals. The results consistently suggested that $E_{M/C}$ varied with soil C/N under different hydrological conditions (Extended Data Fig. 3).

SOM decomposability explains effects of soil C/N on $E_{M/C}$

To explore the potential mechanism of the relationship between $E_{M/C}$ and soil C/N, we collected soil samples from 39 constructed rice paddies along a latitudinal gradient (19.75° N to 47.58° N) (Extended Data Fig. 4). Although these constructed wetland ecosystems cannot represent the magnitude of processes occurring in all natural wetlands, they are useful for isolating specific mechanisms by minimizing the influence of WTD and vegetation[29]. We obtained E_M, E_C and $E_{M/C}$ by measuring CH_4 and CO_2 emissions during anaerobic incubation at a temperature gradient (10, 15, 20, 25 and 30 °C) (Fig. 2a and Supplementary Figs. 2, 3 and 4).

https://doi.org/10.1038/s41561-023-01345-6

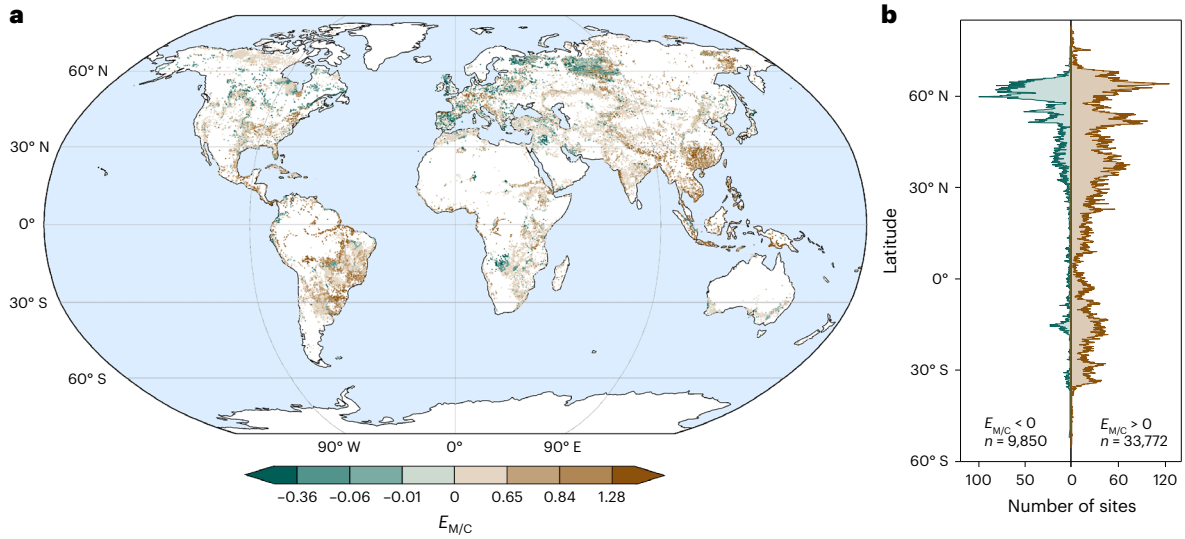

Fig. 3 | Global variations in the temperature dependence of $E_{M/C}$. **a**, Geographical distribution of $E_{M/C}$. This map has a spatial resolution of 30 arcsec (~1 km). There are 43,622 points on this map at a 1 km × 1 km resolution. **b**, Latitudinal distribution of $E_{M/C}$. Yellow represents positive $E_{M/C}$, and green represents negative $E_{M/C}$. *n*, total number of sites.

As expected, soil C/N was significantly negatively correlated with $E_{M/C}$ and acted as an important factor for predicting changes in $E_{M/C}$ (Fig. 2b,c). In addition, the ratio of dissolved organic carbon (DOC) to SOC was significantly positively correlated with $E_{M/C}$ and was an important predictor of changes in $E_{M/C}$. Given that soil C/N and DOC/SOC were significantly correlated ($P < 0.001$) and that they both can indicate SOM decomposability[21,24,30], we speculate that soils with high SOM decomposability have a high $E_{M/C}$ value.

To better characterize the decomposability of SOM, we quantified the apparent activation energy (E_a) of SOM decomposition[31] (Supplementary Fig. 5) and the relative abundance of the carbon molecular functional groups of SOM using solid-state ^{13}C cross-polarization magic-angle-spinning nuclear magnetic resonance spectroscopy[32] (Supplementary Fig. 6). Soils rich in more-active carbon substrates had higher E_M and lower E_C (Extended Data Fig. 5). Thus, $E_{M/C}$ was negatively correlated with the E_a of SOM decomposition, alkyl to alkoxy ratio and degree of aromaticity (Fig. 2d).

The higher alkyl to alkoxy ratio and aromaticity indicated that SOM was more difficult to decompose[32]. According to carbon quality–temperature theory[31], the temperature dependence of CO_2 emissions depends on the E_a of SOM decomposition. These results indicate that E_C may increase with the complexity of the carbon substrate in SOM (Extended Data Fig. 5). In addition, to explore the potential relationship between soil C/N and E_M, we measured the functional gene abundance of *mcrA* (the core gene in the methanogenic pathway, present in all methanogens[33]). The results showed that *mcrA* abundance was negatively correlated with soil C/N (Supplementary Fig. 7). Thus, soils with low C/N ratios may favour the growth and reproduction of methanogenic bacteria. This may facilitate the process of methane production under warming and lead to a higher E_M.

Estimation of global wetland $E_{M/C}$

On the basis of our dataset, we used six machine-learning models, and the light gradient-boosting machine-learning model was finally employed to estimate the variations in seasonal $E_{M/C}$ across the globe with spatial resolutions of 30 arcsec (~1 km) (Methods and Supplementary Fig. 8). Our map showed that $E_{M/C}$ varied from −1.372 to 2.316 across global wetlands, with an average of 0.369 (95% CI: 0.364 to 0.373) (Fig. 3a and Extended Data Fig. 6a). Globally, only 23% of wetlands showed negative $E_{M/C}$ (Fig. 3b).

The hotspots with positive $E_{M/C}$ were distributed across all climatic zones, with the majority in tropical and arid climates (92% and 88%) and the least in cold climates (65%) (Extended Data Fig. 6b). The global $E_{M/C}$ variations were explained mainly by soil C/N (22.7%), whereas averaged WTD accounted for only 0.32% of the variation when estimated by the relative weight analysis of the model ($P < 0.01$). In addition, these results were supported by the lower average soil C/N ratios (12.9 and 11.0) and WTDs (−20.7 cm and −40.5 cm) in the tropical and arid zones than in the cold zones, with an average soil C/N of 18.6 and WTD of −11.7 cm (Extended Data Fig. 6c).

Our results suggest that the relative contribution of CH_4 to greenhouse gas emissions in most wetlands will be stimulated by global warming[3,8]. We should be aware that human activities can change the C/N ratios of wetland soils, which may increase the number of regions where $E_{M/C}$ is positive. For example, the conversion of peatlands to agricultural land[34], loss of coastal wetland vegetation[35] and excessive extraction of underground water[36] can cause a decline in C/N in wetland soils and increased SOM decomposability and $E_{M/C}$ (refs. 37,38). Therefore, efforts to enhance soil carbon sequestration and increase the stable SOC components are likely to decrease the relative contribution of CH_4 to greenhouse gas emissions as well as mitigate wetland greenhouse gas emissions[39].

Taken together, our study highlights the importance of incorporating SOM decomposability into model predictions of global wetland $E_{M/C}$. We found that SOM decomposability had a significant effect on $E_{M/C}$ across global wetlands, and soil C/N can explain more global variations in $E_{M/C}$ than can WTD. Therefore, the absence of SOM decomposability may increase the uncertainties in estimating the relative contribution of wetland CH_4 to global greenhouse gas emissions. It should be noted that soil C/N may be decoupled from SOM decomposability in soils with energy limitations[40] and strong physical protection[41]. Future work is needed to integrate the molecular fingerprinting method and carbon turnover rate[42,43] to comprehensively characterize SOM decomposability and improve the predictions of $E_{M/C}$. Moreover, plant-mediated changes in soil redox potential[44,45], microbial community structure and composition[8,46] and thermal adaptation of microbial physiological metabolism[47] may have cascading but understudied effects on $E_{M/C}$. To advance the understanding of wetland carbon cycling on a warmer Earth, future work is needed to assess the combined effects of soil, plant, hydrologic and climatic conditions on the divergent temperature dependence of greenhouse gas emissions.

Online content

Any methods, additional references, Nature Portfolio reporting summaries, source data, extended data, supplementary information, acknowledgements, peer review information; details of author contributions and competing interests; and statements of data and code availability are available at https://doi.org/10.1038/s41561-023-01345-6.

References

1. Lal, R. Carbon sequestration. *Phil. Trans. R. Soc. B* **363**, 815–830 (2008).
2. Nahlik, A. M. & Fennessy, M. S. Carbon storage in US wetlands. *Nat. Commun.* **7**, 13835 (2016).
3. Chen, H., Xu, X., Fang, C., Li, B. & Nie, M. Differences in the temperature dependence of wetland CO_2 and CH_4 emissions vary with water table depth. *Nat. Clim. Change* **11**, 766–771 (2021).
4. IPCC. *Climate Change 2022: Mitigation of Climate Change* (eds Shukla, P. R. et al.) (Cambbridge Univ. Press, 2022).
5. Mao, S. et al. Aerobic oxidation of methane significantly reduces global diffusive methane emissions from shallow marine waters. *Nat. Commun.* **13**, 7309 (2022).
6. Knoblauch, C., Beer, C., Liebner, S., Grigoriev, M. N. & Pfeiffer, E. M. Methane production as key to the greenhouse gas budget of thawing permafrost. *Nat. Clim. Change* **8**, 309–312 (2018).
7. Segers, R. Methane production and methane consumption: a review of processes underlying wetland methane fluxes. *Biogeochemistry* **41**, 23–51 (1998).
8. Yvon-Durocher, G. et al. Methane fluxes show consistent temperature dependence across microbial to ecosystem scales. *Nature* **507**, 488–491 (2014).
9. Zhao, Q. et al. Soil organic carbon content and stock in wetlands with different hydrologic conditions in the Yellow River Delta, China. *Ecohydrol. Hydrobiol.* **20**, 537–547 (2020).
10. Vicca, S., Janssens, I. A., Flessa, H., Fiedler, S. & Jungkunst, H. F. Temperature dependence of greenhouse gas emissions from three hydromorphic soils at different groundwater levels. *Geobiology* **7**, 465–476 (2009).
11. Lu, B., Song, L., Zang, S. & Wang, H. Warming promotes soil CO_2 and CH_4 emissions but decreasing moisture inhibits CH_4 emissions in the permafrost peatland of the Great Xing'an Mountains. *Sci. Total Environ.* **829**, 154725 (2022).
12. Liu, X. et al. Dynamics and controls of CO_2 and CH_4 emissions in the wetland of a montane permafrost region, northeast China. *Atmos. Environ.* **122**, 454–462 (2015).
13. Matysek, M. et al. Impact of fertiliser, water table, and warming on celery yield and CO_2 and CH_4 emissions from fenland agricultural peat. *Sci. Total Environ.* **667**, 179–190 (2019).
14. Zhao, M. et al. Responses of soil CO_2 and CH_4 emissions to changing water table level in a coastal wetland. *J. Clean. Prod.* **269**, 122316 (2020).
15. Li, Y. et al. Oxygen availability regulates the quality of soil dissolved organic matter by mediating microbial metabolism and iron oxidation. *Glob. Change Biol.* **28**, 7410–7427 (2022).
16. Goncharova, O. Y., Matyshak, G. V., Bobrik, A. A., Timofeeva, M. V. & Sefilyan, A. R. Assessment of the contribution of root and microbial respiration to the total efflux of CO_2 from peat soils and Podzols in the north of Western Siberia by the method of component integration. *Eurasia. Soil Sci.* **52**, 206–217 (2019).
17. Biasi, C., Pitkamaki, A. S., Tavi, N. M., Koponen, H. T. & Martikainen, P. J. An isotope approach based on ^{13}C pulse-chase labelling vs. the root trenching method to separate heterotrophic and autotrophic respiration in cultivated peatlands. *Boreal Environ. Res.* **17**, 184–192 (2012).
18. Maucieri, C., Barbera, A. C., Vymazal, J. & Borin, M. A review on the main affecting factors of greenhouse gases emission in constructed wetlands. *Agric. For. Meteorol.* **236**, 175–193 (2017).
19. Mooshammer, M. et al. Adjustment of microbial nitrogen use efficiency to carbon: nitrogen imbalances regulates soil nitrogen cycling. *Nat. Commun.* **5**, 3694 (2014).
20. Sinsabaugh, R. L., Hill, B. H. & Shah, J. J. F. Ecoenzymatic stoichiometry of microbial organic nutrient acquisition in soil and sediment. *Nature* **462**, 795–798 (2009).
21. Haddix, M. L. et al. The role of soil characteristics on temperature sensitivity of soil organic matter. *Soil Sci. Soc. Am. J.* **75**, 56–68 (2011).
22. Chanton, J. P. et al. Radiocarbon evidence for the substrates supporting methane formation within northern Minnesota peatlands. *Geochim. Cosmochim. Acta* **59**, 3663–3668 (1995).
23. Yuan, F. et al. An integrative model for soil biogeochemistry and methane processes. II: warming and elevated CO_2 effects on peatland CH_4 emissions. *J. Geophys. Res. Biogeosci.* **126**, 2020JG005963 (2021).
24. Wang, Q., Liu, S. & Tian, P. Carbon quality and soil microbial property control the latitudinal pattern in temperature sensitivity of soil microbial respiration across Chinese forest ecosystems. *Glob. Change Biol.* **24**, 2841–2849 (2018).
25. Allen, A. P., Gillooly, J. F. & Brown, J. H. Linking the global carbon cycle to individual metabolism. *Func. Ecol.* **19**, 202–213 (2005).
26. Enquist, B. J. et al. Scaling metabolism from organisms to ecosystems. *Nature* **423**, 639–642 (2003).
27. Zuur, A. F., Ieno, E. N., Walker, N. J., Saveliev, A. A. & Smith, G. M. *Mixed Effects Models and Extensions in Ecology with R* (Springer, 2009).
28. Yvon-Durocher, G. et al. Reconciling the temperature dependence of respiration across timescales and ecosystem types. *Nature* **487**, 472–476 (2012).
29. Xiang, D., Wang, G., Tian, J. & Li, W. Global patterns and edaphic-climatic controls of soil carbon decomposition kinetics predicted from incubation experiments. *Nat. Commun.* **14**, 2171 (2023).
30. Bosatta, E. & Agren, G. I. Soil organic matter quality interpreted thermodynamically. *Soil Biol. Biochem.* **31**, 1889–1891 (1999).
31. Davidson, E. A. & Janssens, I. A. Temperature sensitivity of soil carbon decomposition and feedbacks to climate change. *Nature* **440**, 165–173 (2006).
32. Hall, S. J., Ye, C. L., Weintraub, S. R. & Hockaday, W. C. Molecular trade-offs in soil organic carbon composition at continental scale. *Nat. Geosci.* **13**, 687–692 (2020).
33. Evans, P. N. et al. An evolving view of methane metabolism in the Archaea. *Nat. Rev. Microbiol.* **17**, 219–232 (2019).
34. Temmink, R. J. M. et al. Recovering wetland biogeomorphic feedbacks to restore the world's biotic carbon hotspots. *Science* **376**, eabn1479 (2022).
35. Wang, Z. G. et al. Human-induced erosion has offset one-third of carbon emissions from land cover change. *Nat. Clim. Change* **7**, 345–349 (2017).
36. Liu, L. et al. Water table drawdown reshapes soil physico-chemical characteristics in Zoige peatlands. *Catena* **170**, 119–128 (2018).
37. Leifeld, J., Klein, K. & Wust-Galley, C. Soil organic matter stoichiometry as indicator for peatland degradation. *Sci. Rep.* **10**, 7634 (2020).
38. Leifeld, J. & Menichetti, L. The underappreciated potential of peatlands in global climate change mitigation strategies. *Nat. Commun.* **9**, 1071 (2018).
39. Evans, C. D. et al. Overriding water table control on managed peatland greenhouse gas emissions. *Nature* **593**, 548–552 (2021).
40. Hoffland, E., Kuyper, T. W., Comans, R. N. J. & Creamer, R. E. Eco-functionality of organic matter in soils. *Plant Soil* https://doi.org/10.1007/s11104-020-04651-9 (2020).

41. Billings, S. A. & Ballantyne, F. How interactions between microbial resource demands, soil organic matter stoichiometry, and substrate reactivity determine the direction and magnitude of soil respiratory responses to warming. *Glob. Change Biol.* **19**, 90–102 (2013).
42. Cotrufo, M. F. et al. Formation of soil organic matter via biochemical and physical pathways of litter mass loss. *Nat. Geosci.* **8**, 776–779 (2015).
43. Koven, C. D., Lawrence, D. M. & Riley, W. J. Permafrost carbon-climate feedback is sensitive to deep soil carbon decomposability but not deep soil nitrogen dynamics. *Proc. Natl Acad. Sci. USA* **112**, 3752–3757 (2015).
44. Noyce, G. L., Smith, A. J., Kirwan, M. L., Rich, R. L. & Megonigal, J. P. Oxygen priming induced by elevated CO_2 reduces carbon accumulation and methane emissions in coastal wetlands. *Nat. Geosci.* **16**, 63–68 (2023).
45. Leroy, F. et al. Vegetation composition controls temperature sensitivity of CO_2 and CH_4 emissions and DOC concentration in peatlands. *Soil Biol. Biochem.* **107**, 164–167 (2017).
46. Fey, A. & Conrad, R. Effect of temperature on carbon and electron flow and on the archaeal community in methanogenic rice field soil. *Appl. Environ. Microbiol.* **66**, 4790–4797 (2000).
47. Bradford, M. A. et al. Thermal adaptation of soil microbial respiration to elevated temperature. *Ecol. Lett.* **11**, 1316–1327 (2008).

Methods

Compilation of the global database

Using the Web of Science (http://apps.webofknowledge.com), Google Scholar (https://scholar.Google.com) and the China National Knowledge Infrastructure Database (http://www.cnki.net), we searched for all peer-reviewed articles on CO_2 and CH_4 emissions from wetland soils published before 20 July 2023. The keywords were 'wetland' and 'greenhouse gas emissions'. To prevent bias in publication selection, the data were screened on the basis of the following criteria. (1) Greenhouse gas emissions were measured in the field. (2) To better quantify the temperature dependence of greenhouse gas emissions, only data with at least three different temperatures were included. (3) The ecosystem was identified as a wetland in the Ramsar Convention[48] (an area of marsh, peatland or water, whether natural or artificial, permanent or temporary, with water that is static or flowing, fresh, brackish or saltwater, including an area of seawater not exceeding six metres in depth at low tide). (4) Only control or undisturbed plots were included. (5) The duration of the study was at least three months to avoid short-term disturbance. Data on greenhouse gas emissions, temperature, latitude and longitude, SOC, total nitrogen (TN), total phosphorus (TP), soil texture (clay, silt and sand contents), mean annual temperature, mean annual precipitation, mean annual evaporation and WTD were extracted from the eligible literature. In addition, for some observations, the soil, climatic or hydrological variables were not reported in the text. We filled in the missing data using the following global databases. Global soil data were obtained from the gridded Global Soil Dataset at a 0.083° spatial resolution[49]. The climatic data from 1970 to 2000 (spatial resolution of 30 arcsec) were obtained from the WorldClim database version 2 (https://www.worldclim.org/data/worldclim21.html). Wetland water-table depth was obtained from the European Union collaborative project of Global Water Science Information Service (https://glowasis.deltares.nl/thredds/catalog/opendap/opendap/Equilibrium_Water_Table/catalog.html)[50]. The software GetData (v.2.22) was used to extract data from the graph.

Quantification of the apparent activation energy of CH_4 and CO_2 emissions

The LME model was used to quantify the temperature dependence of CH_4 and CO_2 emissions. The model allows for nested covariance structures, especially site-level relationships nested within overall relationships[3,51,52]. It addresses unbalanced designs when measuring CH_4 and CO_2 emissions in the field. For example, the number of measurements of CH_4 and CO_2 emissions varies from study to study. The LME model can reduce the impact of fixed effects (generally temperature) on CH_4 and CO_2 emissions since the study site is regarded as a random effect. Therefore, the LME model has been widely used to study the temperature dependence of greenhouse gas emissions[3,8].

The temperature dependence of CO_2 and CH_4 emissions was quantified on the basis of the Boltzmann–Arrhenius function as follows[3,8]:

$$\ln R_i(T) = (E + \epsilon_E^i)\left(\frac{1}{kT_C} - \frac{1}{kT}\right) + \ln R(T_C) + \epsilon_R^i$$

where $\ln R_i(T)$ represents the natural logarithm of the CO_2 or CH_4 emissions at absolute temperature (in Kelvin) for site i; E is the average apparent activation energy across sites, which characterizes the temperature dependence of CH_4 and CO_2 from wetlands; and k is the Boltzmann constant (8.62×10^{-5} eV K^{-1}). ϵ_E^i and ϵ_R^i represent the bias for a particular site i. We normalize the temperature data using the average temperature T_C in the database; thus, $\ln R(T_C)$ corresponds to the average emission rate among sites at T_C. When site i does not contain the temperature T_C, the site is normalized separately. Because the response of CH_4 and CO_2 emissions to temperature may vary significantly depending on the site, we consider the site as a random effect and the temperature as a fixed effect. The slope of the fitted equation is regarded as the apparent activation energy[3,8]. The LME model analysis was performed with the 'lmer' function in the 'lme4' package in R statistical software (v.3.6.3)[3,53].

To determine whether it was necessary to include random effects corresponding to the variations in both slope and intercept among sites and seasons, we assessed the improvement in model fit between the null model (no random effect) and three alternative models (random effect on the intercept only, random effect on the slope only and random effect on the slope and intercept). By comparing the Akaike information criterion values of these models (Supplementary Table 1), we found that the random-effects structure that best described each database included random variation in both the slope and intercept. Therefore, we applied a random-effects structure including random variation in both the slope and intercept to assess the significance of the fixed effects (averages across sites for the apparent activation energy and intercept). We used the confidence interval overlap method to compare the slopes and intercepts generated from different mixed-effects models[54].

The apparent activation energy of carbon emissions was characterized using the LME model after fitting the Boltzmann–Arrhenius function to the data of the carbon emissions and the standardized temperature. We set the carbon emissions as the dependent variable, the temperature as the fixed effect and site as a random effect in the LME model. The regression slope was the apparent activation energy of carbon emissions. Carbon emissions were expressed in standardized form as $\ln[R_i(T_i)/R_i(T_C)]$, where $R_i(T_i)$ is the measured CO_2/CH_4 emissions ratio at site i, and $R_i(T_C)$ is the site-specific estimate of the CO_2/CH_4 emissions ratio at a fixed temperature (the average measured temperature in the database). The normalization temperature is $1/kT_C - 1/kT$, where k is the Boltzmann constant (8.62×10^{-5} eV K^{-1}).

Partition of soil C/N intervals

We used a sliding window analysis to partition the soil C/N intervals in our global database. We hypothesized that there was a threshold i to distinguish the positive and negative $E_{M/C}$ values. Following this hypothesis, we divided the CH_4 and CO_2 emissions data into two groups according to soil C/N ≤ i (Group I) and soil C/N > i (Group II). We used the enumeration method to identify each assumed i (i = 1, 2, 3 … (in steps of 1)). The results showed that when i was less than 12, the $E_{M/C}$ value of Group I was positive, but it could not be significantly fitted in Group II ($P > 0.05$ in LME models); when i was between 12 and 21, the $E_{M/C}$ value of Group I was positive and the $E_{M/C}$ value of Group II was negative; and when i was more than 21, the $E_{M/C}$ value of Group II was negative, but it could not be significantly fitted in Group I ($P > 0.05$ in LME models). We found that the threshold i was not a fixed value and ranged from 12 to 21 across global wetlands. Therefore, we can divide the greenhouse gas emissions data in our global database into three intervals according to soil C/N ≤ 12 (Group I), > 12 and ≤ 21 (the range of threshold i) (Group II). Refer to Supplementary Table 2 for the process and detailed information.

Soil sample collections in constructed rice paddies in China

In total, we collected 429 soil samples (13 regions × 3 sites × 11 replicates). The soils were collected from 13 regions in China's main growing regions: Hailun, Changchun, Shenyang, Yuanyang, Fengqiu, Lin 'an, Quzhou, Zixi, Jian'ou, Changting, Hengyang, Qingxin and Haikou (Extended Data Fig. 4a), which covered five climatic zones from North China to South China (cold temperate zone, middle temperate zone, warm temperate zone, subtropical zone and tropical zone). These regions had great latitudinal (from 19.75° N to 47.58° N) and climatic (the mean temperature during the rice growing season varied from 16.0 to 27.8 °C) variability. These differences resulted in great variation in soil C/N (from 9.2 to 14.5) among different regions, which was conducive to us observing the relationship between soil C/N and the $E_{M/C}$ values. Three paddy sites were selected in each region. To ensure the

similarity of the climate, soil type and farming practices of the selected study sites, the three sites in the same region were located within 20 km. Eleven soil samples were collected from a 100 m × 100 m plot using a spatially explicit 'L-shaped' sampling design at each site (Extended Data Fig. 4b). At each sampling point, five soil cores (2.5 cm in diameter) from the upper 15 cm were taken and mixed thoroughly, and any visible living plant material (for example, roots) was manually removed from the composite soil sample. The soil samples were transported to the laboratory on dry ice. Subsamples were stored at 4 °C to measure the soil geochemical variables. Furthermore, the DOC, dissolved organic nitrogen, SOC, TN, TP, ammonium nitrogen (NH_4^+-N), nitrate nitrogen (NO_3^-N), ratio of ammonium nitrogen to nitrate nitrogen (NH_4^+/NO_3^-N), available phosphorus, total potassium, available potassium, pH and cation exchange capacity of these soils were measured.

Apparent activation energy of CH_4 emissions (E_M) and CO_2 emissions (E_C)

We placed 20 g of fresh soil into a 100 ml flask (three flasks per paddy soil, $n = 3$) and then vacuumed out all the air in the flask. We then purged with N_2 repeatedly to remove residual O_2, CO_2 and CH_4. The soil samples were completely flooded with anoxic distilled water and incubated in darkness at 10, 15, 20, 25 and 30 °C (±0.5 °C) for 28 days. Gas samples were taken with a pressure-lock syringe after the flasks were heavily shaken by hand and analysed for CH_4 and CO_2 with a gas chromatography–flame ionization detector. We then fitted a Boltzmann–Arrhenius function to the CH_4 and CO_2 emissions using the LME models to assess E_M and E_C (ref. 3).

Apparent activation energy of SOM decomposition

To characterize the decomposability of SOM, we quantified the apparent activation energy (E_a) of SOM decomposition because SOM that is difficult to decompose usually has a higher E_a. The E_a of SOM decomposition can be characterized by the temperature dependence of the reaction rate of SOM mineralization to CO_2 under aerobic conditions[31]. Specifically, 20 g of fresh soil samples from 13 regions were placed in a 50 ml flask. The water content of the soils in these tubes was adjusted to 60% of the field water-holding capacity before conducting the incubation[55]. A CO_2 trap (20 ml of 2 mol l^{-1} NaOH in a 50 ml tube to absorb the CO_2 produced), a tube of deionized water (20 ml water in a 50 ml tube to maintain constant humidity) and three tubes of soil were placed in each incubation bucket. The incubation bucket was a 1 l black plastic jar, and three incubation buckets were conducted per paddy soil ($n = 3$). Triplicate blank buckets containing only the CO_2 trap and deionized water were also incubated to account for the headspace of CO_2. After the 1st, 3rd, 6th, 10th, 15th, 21st and 28th days of incubation, the CO_2 emissions were determined by titration with 1 mol l^{-1} HCl using 1% phenolphthalein and methyl orange as the pH indicator. We then fitted a Boltzmann–Arrhenius function to the CO_2 emissions data using the LME models to assess the E_a of SOM decomposition[3].

Molecular structure of the carbon substrate in SOM

We quantified the relative abundance of the carbon molecular functional groups of SOM to characterize the decomposability of SOM. Specifically, we used solid-state ^{13}C cross-polarization magic-angle-spinning nuclear magnetic resonance (^{13}C-CPMAS NMR) spectra to characterize the organic carbon molecular composition. In addition, to improve the NMR sensitivity and remove paramagnetic species, soils were pretreated with hydrofluoric acid (10% wt) to prevent interference of Fe^{3+} and Mn^{2+}. Briefly, 5 g of finely ground soil was weighed into a 100 ml sealed polyethylene centrifugation tube, saturated with 50 ml hydrofluoric acid and shaken for 1 h. Subsequently, the slurry was centrifuged at 1,000 times gravity for 10 min (3,000 r min^{-1} using Centrifuge 5804 R), and the supernatant was removed and discarded appropriately. After repeating this procedure eight times, each sample was washed with distilled water four times, dried at 40 °C under a stream of dinitrogen gas, pulverized through a 60-mesh sieve and reserved for NMR[56].

We recorded ^{13}C-CPMAS NMR spectra at room temperature (23 °C) using an AVANCE II 300MH with a 7 mm CPMAS probe. The observation frequency was set to 100.5 MHz, and the rotation frequency of the magic-angle spinning was set to 5,000 Hz. The contact time was set to 2 ms, and the cycle delay time was 1.2 s. Composite pulse proton decoupling was applied during signal acquisition. After baseline correction, quantification was performed by dividing the spectra into seven chemical shift regions: 0-45 ppm, 45–60 ppm, 60–95 ppm, 95–110 ppm, 110–145 ppm, 145–160 ppm and 160–220 ppm, assigned to alkyl C, N-alkyl + methoxyl C, O-alkyl C, Di-O-alkyl C, aromatic C, phenolic C and amide + carbonyl C, respectively. We used the ratio of alkyl to alkoxy carbons and the degree of aromaticity to quantify the decomposability of SOM. Ratio of alkyl carbon to alkoxy carbon = alkyl C/(O-alkyl C + N-alkyl + methoxyl C + Di-O-alkyl C). Degree of aromaticity = (aromatic C + phenolic C)/[1 − (amide + carbonyl C)].

Quantification of *McrA* gene abundance

McrA is the core gene encoding methyl coenzyme M reductase, which can reduce methyl coenzyme M to form methane and catalyse the last step of methane production. The *mcrA* gene is present in all methanogens, so the abundance of the *mcrA* gene can be used as a key indicator to measure the methanogenic capacity of microbial communities[33]. To qualify the *McrA* abundance, we used a QIAquick Purification kit (Qiagen) to purify 600 ng soil DNA from each sample and labelled DNA with the fluorescent dye Cy-3 (GE Healthcare) using random primers[57]. The labelled gDNA was dried and rehydrated with 2.7 μg of a sample-tracking control, followed by incubation at 50 °C for 5 min. The DNA solution was mixed with hybridization solution containing 1× Acgh blocking, 10 pM universal standard DNA, 1× HI-RPM hybridization buffer, 0.05 μg μl^{-1} Cot-1 DNA and 10% formamide (final concentrations). Then the solution was denatured at 95 °C for 3 min, incubated at 37 °C for 30 min and hybridized with GeoChip 5.0 arrays (180 K). The microarray data were preprocessed by the microarray analysis pipeline on the Institute for Environmental Genomics website (http://ieg.ou.edu/microarray/)[58]. The spots of poor quality with a signal-to-noise ratio less than 2.0 were removed after normalization. The relative abundance of each soil sample was calculated by dividing by the total intensity of the detected probes, multiplying by a constant and taking the natural logarithm transformation. Only probes detected in more than two out of eight samples from the same sampling site were retained.

Mapping of the global distribution of $E_{M/C}$

To predict the spatial variations in $E_{M/C}$, we used the site-level $E_{M/C}$ as the dependent variable and ten soil variables (SOC, TN, TP, soil C/N, C/P, N/P, pH, clay content, silt content and sand content), four climatic variables (mean annual temperature, mean annual precipitation, mean annual evaporation and aridity index), latitude and mean annual WTD as independent variables. To identify the best model for predicting the global variations in $E_{M/C}$, we selected four normal machine-learning models (the random forest model, the extreme gradient-boosting model, the light gradient-boosting machine model and the gradient-boosting decision trees model) and two deep machine-learning models (convolutional neural networks and deep neural networks). The data used for training and validation are 80% and 20%, respectively. Self-organizing maps for synthetic data generation were used to enhance the performance and accuracy of the models. For these models, we evaluated the strength of the prediction using the mean absolute errors, the mean square errors and the coefficient of determination (R^2). The results showed that the light-gradient boosting machine model performed best among all models (Supplementary Fig. 8) and was therefore selected to predict the global variations in $E_{M/C}$. All models were run in Python.

Data availability

All data needed to evaluate the conclusions are available at Zenodo (https://zenodo.org/records/10044208). The GeoChip data are available in the repository Figshare (https://doi.org/10.6084/m9.figshare.9746303). Source data are provided with this paper.

Code availability

The code used in this study is archived in Supplementary Code 1 and is available at Zenodo (https://zenodo.org/records/10044208).

References

48. Matthews, G. V. T. *The Ramsar Convention on Wetlands: Its History and Development* (Ramsar Convention Bureau, 1993).
49. Shangguan, W., Dai, Y. J., Duan, Q. Y., Liu, B. Y. & Yuan, H. A global soil data set for Earth system modeling. *J. Adv. Model. Earth Syst.* **6**, 249–263 (2014).
50. Fan, Y., Li, H. & Miguez-Macho, G. Global patterns of groundwater table depth. *Science* **339**, 940–943 (2013).
51. Sun, Y. et al. A global meta-analysis on the responses of C and N concentrations to warming in terrestrial ecosystems. *Catena* **208**, 105762 (2022).
52. Liu, Y., Jiang, M., Lu, X., Lou, Y. & Liu, B. Carbon, nitrogen and phosphorus contents of wetland soils in relation to environment factors in Northeast China. *Wetlands* **37**, 153–161 (2017).
53. R Core Team. *R: A Language and Environment for Statistical Computing (Version 3.6.3)* (R Foundation for Statistical Computing, 2020); http://www.r-project.org
54. Payton, M. E., Greenstone, M. H. & Schenker, N. Overlapping confidence intervals or standard error intervals: what do they mean in terms of statistical significance? *J. Insect Sci.* **3**, 34 (2003).
55. Zhong, Z. et al. Adaptive pathways of soil microorganisms to stoichiometric imbalances regulate microbial respiration following afforestation in the Loess Plateau, China. *Soil Biol. Biochem.* **151**, 108048 (2020).
56. Gelinas, Y., Baldock, J. A. & Hedges, J. I. Demineralization of marine and freshwater sediments for CP/MAS ^{13}C NMR analysis. *Org. Geochem.* **32**, 677–693 (2001).
57. Liang, Y. et al. Development of a common oligonucleotide reference standard for microarray data normalization and comparison across different microbial communities. *Appl. Environ. Microbiol.* **76**, 1088–1094 (2010).
58. Shi, Z. et al. Functional gene array-based ultrasensitive and quantitative detection of microbial populations in complex communities. *mSystems* **4**, e00296-19 (2019).

Acknowledgements

The authors received funding from Strategic Priority Research Program of the Chinese Academy of Sciences (XDA28030102 to Y.L.), National Natural Scientific Foundation of China (92251305 to M.N., 41622104 to Y.L.), Innovation Program of the Institute of Soil Science (ISSASIP2201 to Y.L.) and Youth Innovation Promotion Association of the Chinese Academy of Sciences (2016284 to Y.L.).

Author contributions

Y.L., H.H., M.N., J.C. and J. Zhang conceptualized the research project. H.H., M.N., M.D.-B., H.N., F.Z., J. Zhou and Y.L. developed the methodology. H.H., J.C., M.D.-B., H.N., W.H., X.S., H.L. and Y.L. were responsible for data collection and analysis. Y.L., J. Zhang, X.C. and B.S. provided supervision throughout the project. Y.L., H.H., J.C., M.N., D.H. and T.W.C. wrote the original draft. H.H., J.C., F.Z., M.N., D.H., H.L., M.D.-B., H.N., W.H., J. Zhou, X.S., X.C., B.S., J. Zhang, T.W.C. and Y.L. contributed to the review and editing process.

Competing interests

The authors declare no competing interests.

Additional information

Extended data is available for this paper at https://doi.org/10.1038/s41561-023-01345-6.

Supplementary information The online version contains supplementary material available at https://doi.org/10.1038/s41561-023-01345-6.

Correspondence and requests for materials should be addressed to Yuting Liang.

Peer review information *Nature Geoscience* thanks the anonymous reviewers for their contribution to the peer review of this work. Primary Handling Editor: Xujia Jiang, in collaboration with the *Nature Geoscience* team.

https://doi.org/10.1038/s41561-023-01345-6

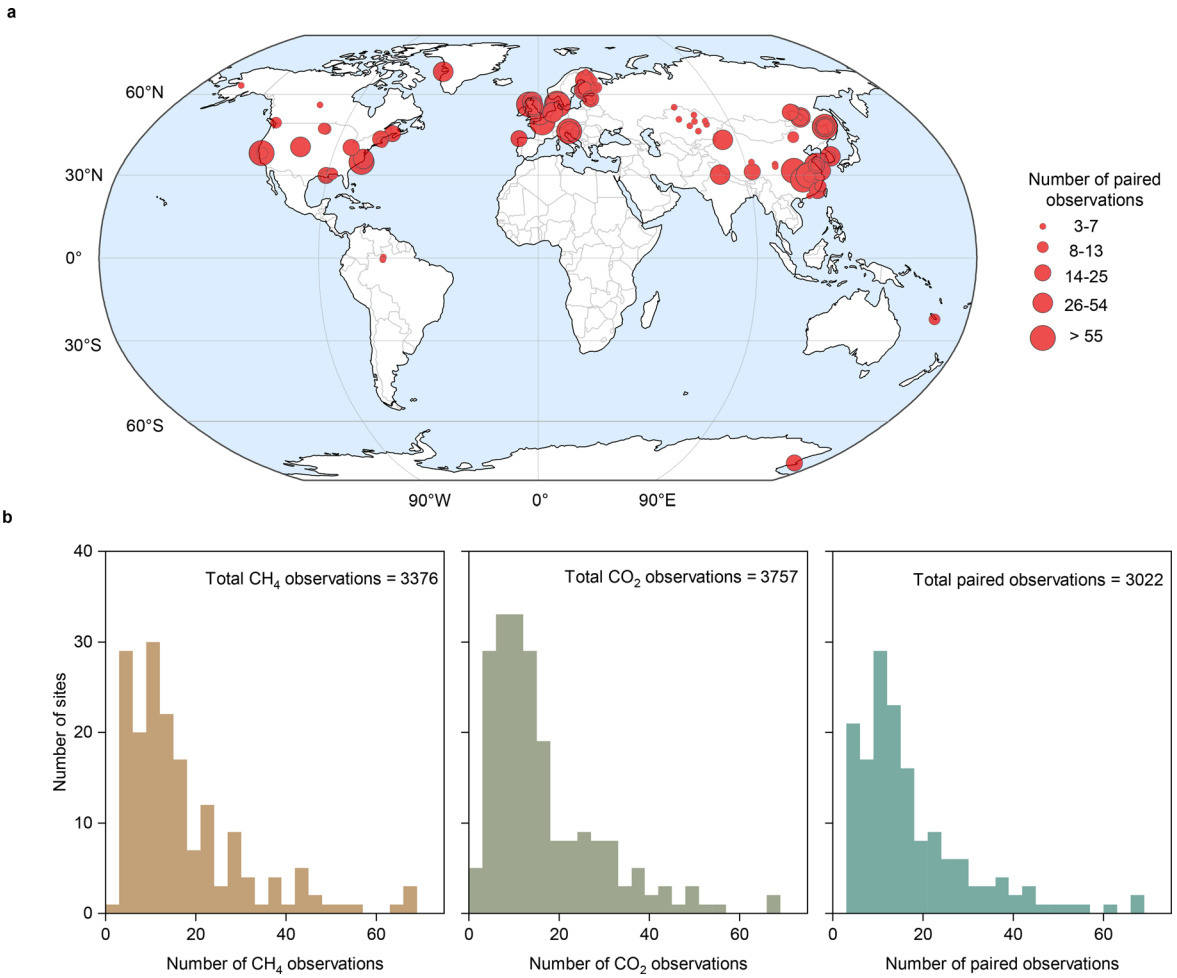

Extended Data Fig. 1 | Geographical distribution of the sites in the global database (a) and frequency distribution of carbon emission observations at the site level (b). In panel a, there might be overlaps among these sites. The size of the circle indicates the number of observations.

https://doi.org/10.1038/s41561-023-01345-6

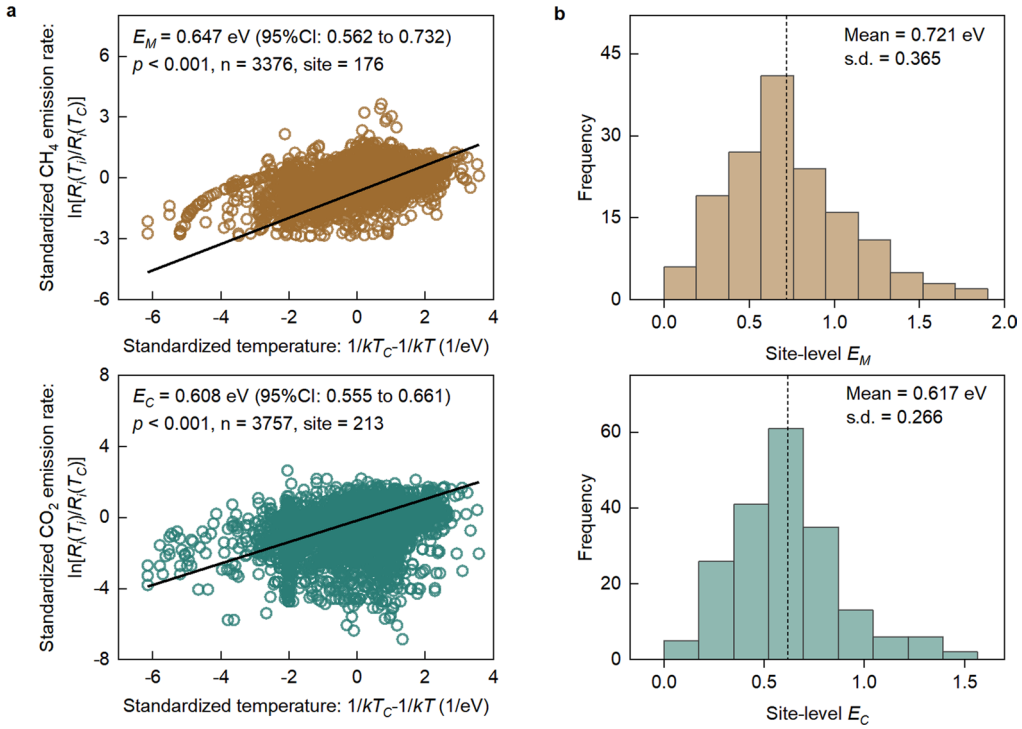

Extended Data Fig. 2 | Temperature dependence of CO_2 (E_C) and CH_4 (E_M) emissions on a global scale. a, The temperature dependence of the greenhouse gas (GHG) emissions was characterized using the linear mixed effects (LME) model after fitting the Boltzmann-Arrhenius function to the data of the GHG emissions and the standardized temperature (Methods). **b**, The dashed lines show the average.

https://doi.org/10.1038/s41561-023-01345-6

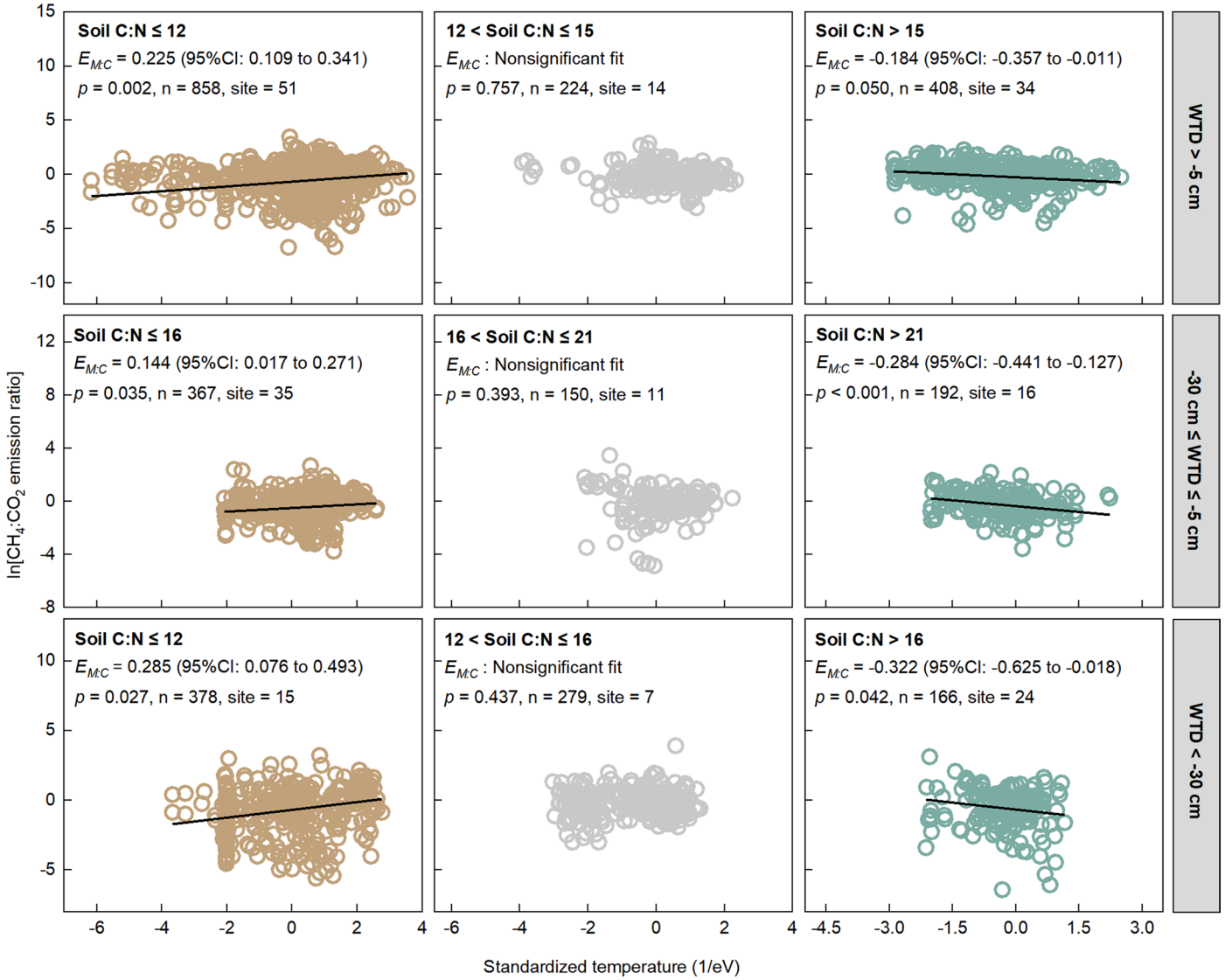

Extended Data Fig. 3 | Temperature dependence of the CH_4:CO_2 emission ratio ($E_{M:C}$) at different water table depth intervals and soil C:N intervals. The temperature dependence was characterized using the linear mixed effects (LME) model after fitting the Boltzmann-Arrhenius function to the data of the CH_4:CO_2 emission ratio and the standardized temperature (Methods). Different soil C:N intervals were classified using the results of the sliding window-LME model. Different water table depth intervals are classified according to the results of Chen *et al.* (ref. 3, 10.1038/s41558-021-01108-4).

https://doi.org/10.1038/s41561-023-01345-6

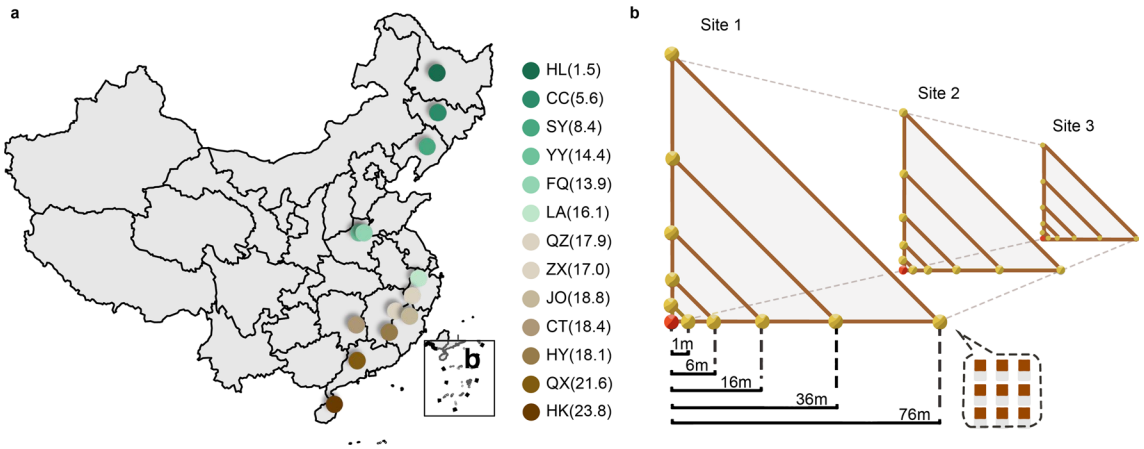

Extended Data Fig. 4 | Geographical distribution of the sites (a) and sampling strategy (b) in the incubation experiment. Samples were taken from 39 paddy soil sites located in 13 regions of China. The numbers in parentheses represent the mean annual air temperature (°C) in the sampling region. At each site, 11 nested samples were collected at distances of 1, 6, 16, 36 and 76 m. CC = Changchun; CT = Changting; FQ = Fengqiu; HK = Haikou; HL = Hailun; HY = Hengyang; JO = Jian'ou; LA = Lin'an; OM = organic matter; QX = Qingxin; QZ = Quzhou; SY = Shenyang; TN = total nitrogen; YY = Yuanyang; ZX = Zixi.

https://doi.org/10.1038/s41561-023-01345-6

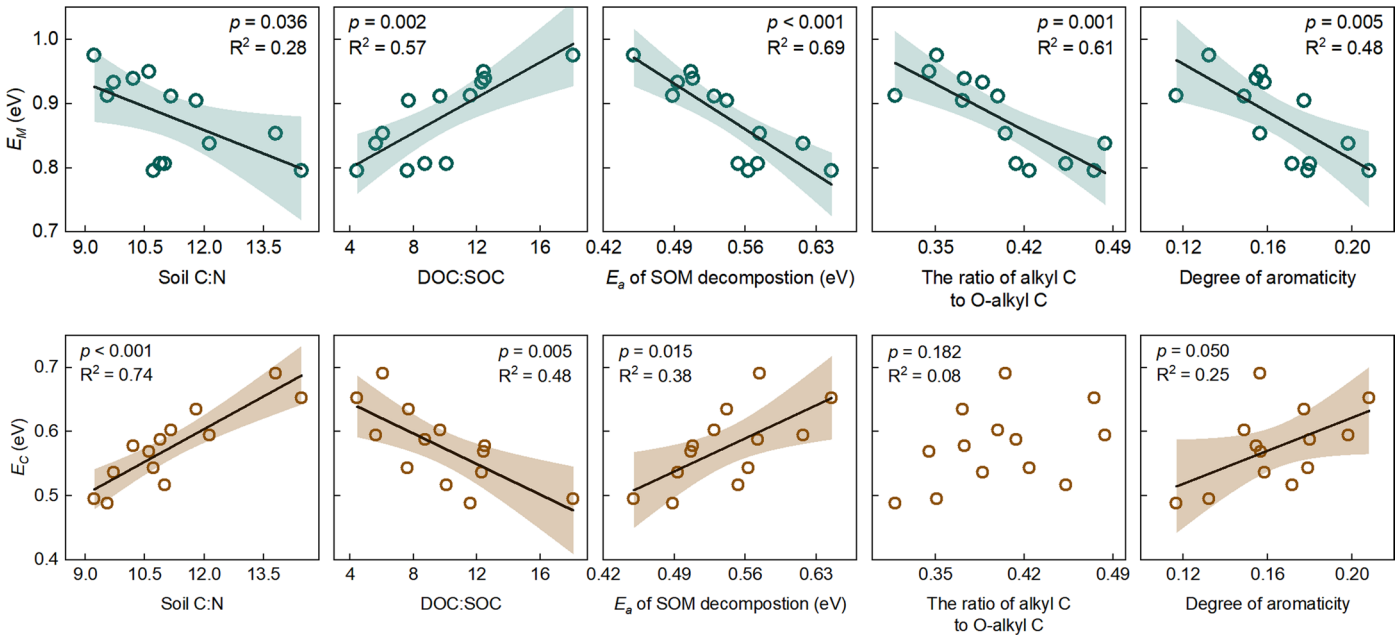

Extended Data Fig. 5 | Linear regression analysis between the temperature dependences of CH_4 emissions (E_M) and CO_2 emissions (E_C) with soil organic matter decomposability in incubation experiments. The E_a of SOM decomposition represents the apparent activation energy of soil organic matter decomposition. DOC, dissolved organic carbon; SOC, soil organic carbon. Error bands are 95% confidence intervals of the regression lines.

https://doi.org/10.1038/s41561-023-01345-6

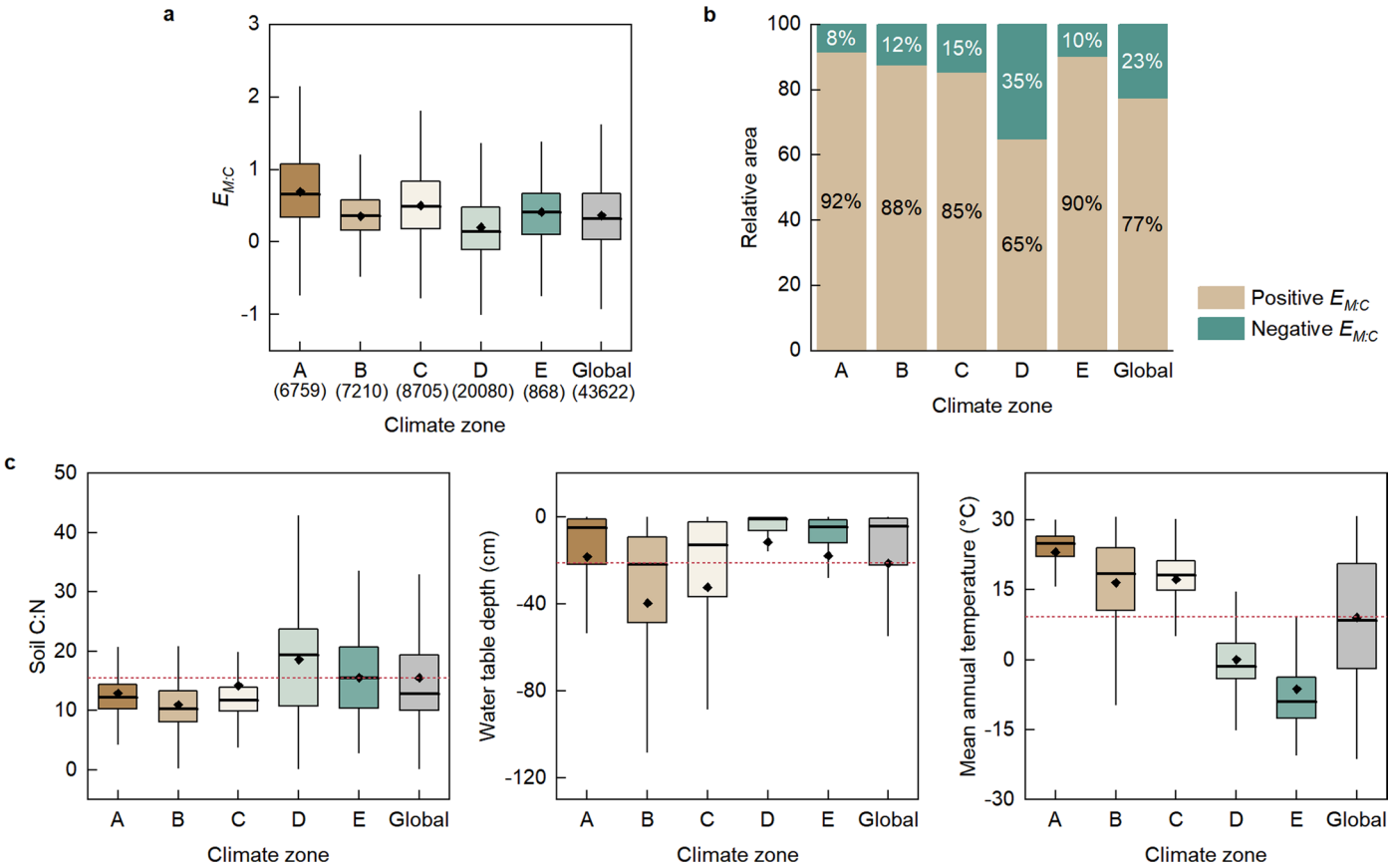

Extended Data Fig. 6 | The distribution of the difference in the temperature dependence of CH_4 and CO_2 emissions ($E_{M:C}$), soil C:N, water table depth, and mean annual temperature in different climate zones. a, $E_{M:C}$ distribution in different climate zones. The climatic zones are classified by the Köppen climate classification. A, B, C, D, and E represent tropical, arid, temperate, cold, and polar climates, respectively. Centre lines are medians, and diamonds represent the averages. Box limits are upper and lower quartiles. whiskers are 1.5× the interquartile ranges. The numbers in brackets represent wetland area (km^2). **b**, Relative area of wetlands with positive and negative $E_{M:C}$ values. **c**, The distribution of soil, water table depth, and mean annual temperature of wetlands in different climate zones. The red dotted lines are the global mean values.